RADIATION EFFECTS ON CMOS PARTICLE DETECTORS

JERNEJ DEBEVC

Fakulteta za matematiko in fiziko
Univerza v Ljubljani

In particle physics experiments, silicon detectors usually constitute an essential part of the vertexing and tracking systems, situated closest to the interaction point. The products of particle collisions induce significant radiation damage in the detector material, which has to be well understood and accounted for to retain adequate performance throughout the detector lifetime. This article presents radiation damage in silicon and its effects on particle detectors, together with measurements of depletion properties of CMOS monolithic prototype detectors considered as an option for installation in the ATLAS Pixel Detector using the Edge-TCT technique.

UČINKI SEVANJA NA CMOS DETEKTORJE DELCEV

Pri eksperimentih na področju fizike osnovnih delcev silicijevi detektorji s svojo osrednjo postavitvijo najbližje interakcijski točki pogosto predstavljajo najpomembnejši del sledilnega sistema. Visokoenergijski delci, ki nastanejo pri interakcijah, v materialu detektorjev povzročijo veliko sevalnih poškodb, katere je potrebno dobro razumeti in upoštevati, da zagotovimo zanesljivo delovanje detektorja čez celotno predvideno življenjsko dobo. Ta članek predstavi glavne učinke sevanja v siliciju in njihove posledice za delovanje detektorjev delcev ter meritve lastnosti osiromašenega področja s tehniko Edge-TCT na monolitnih CMOS prototipih detektorjev, ki so bili obravnavani za potencialno uporabo v detektorju ATLAS.

1. Introduction

In the field of particle physics, large detectors measuring particles resulting from highly energetic collisions are the main instruments used for determining the properties of particles, their interactions and searching for new physics beyond the Standard Model (SM). The extreme energy of these collisions and the high collision rates produce an exceptionally harsh radiation environment in which these detectors are required to operate. Ensuring adequate performance of all detector components throughout the detector lifetime is therefore of vital importance. For this reason, an appreciable amount of effort has to be devoted to research and development of these components to fulfill the desired performance requirements and to understand their properties in detail.

One of the important factors that has to be considered when designing detector elements is their resistance to radiation caused by particles created in collisions traveling through the detector material. Understanding the effect of radiation on crucial components prior to their installation ensures that their electrical and structural properties remain acceptable for the entire expected period of operation. This is especially important for components located close to the interaction point, where particle fluxes are the largest.

This article focuses on radiation effects in CMOS particle detectors that have been studied as a possibility for use in the new tracking system of the ATLAS detector at the Large Hadron Collider (LHC). Firstly, the upcoming ATLAS detector upgrade is presented in connection with the CMOS detector option, followed by a general discussion of radiation effects in silicon and its consequences. Finally, the experimental setup used for determining detector properties is presented.

2. ATLAS detector and upgrade for HL-LHC

The ATLAS detector [1] at the Large Hadron Collider has delivered numerous important results over the past decade at the currently achievable limits of the high energy frontier. It continues to verify the predictions of the SM and hopes to answer open questions about dark matter and physics beyond the Standard Model, such as supersymmetry. In order to increase the potential for new

discoveries and to improve the statistics, the LHC is currently scheduled for an upgrade starting in 2024 which will increase its design luminosity $\mathcal{L}$ [2], the quantity connecting the event rate $\mathrm{d}N/\mathrm{d}t$ to the cross section of the interaction σ

$$\frac{\mathrm{d}N}{\mathrm{d}t} = \mathcal{L}\,\sigma\,. \tag{1}$$

This expression can be integrated with respect to time to get the cumulative number of events, which is proportional to the integrated luminosity

$$\mathcal{L}_{\mathrm{int}} = \int \mathcal{L}\,\mathrm{d}t\,. \tag{2}$$

The current nominal luminosity of the LHC is $10^{34}\,\mathrm{cm}^{-2}\,\mathrm{s}^{-1}$, however, due to excellent performance of the accelerator, $2\cdot10^{34}\,\mathrm{cm}^{-2}\,\mathrm{s}^{-1}$ was achieved in 2018. With these values, the present goal is to collect a total of $\mathcal{L}_{\mathrm{int}} = 350\,\mathrm{fb}^{-1}$ before the start of the upgrade period. After the upgrade project, named High-Luminosity Large Hadron Collider (HL-LHC), the peak luminosity will be increased to $5\cdot10^{34}\,\mathrm{cm}^{-2}\,\mathrm{s}^{-1}$, accumulating up to $3000\,\mathrm{fb}^{-1}$ of integrated luminosity over the following years of operation [2].

To cope with the increase in luminosity, the ATLAS detector will undergo an upgrade as well, called the Phase-II upgrade [3]. In its current configuration, the detector is unsuitable for operation in the high event rate environment of the HL-LHC. A higher event rate results in larger particle fluxes throughout the detector. For the tracking system this means a higher hit and data rate, which are beyond the capabilities of the current setup. Furthermore, the sensors would not withstand the additional radiation damage, causing degradation of performance beyond the point of usability. Therefore, among other improvements, the Phase-II upgrade will see the entire current tracking system of the detector replaced with the new Inner Tracker (ITk).

2.1 ATLAS Inner Tracker

The new Inner Tracker (Fig. 1) will feature an all-silicon design divided into two main subsystems, differing in the type of silicon sensors being used.

In the outer layers, the Strip Detector [5] will hold silicon sensors with individual pixels elongated in one direction and therefore resembling strips. These will be from $18\,\mathrm{mm}$ to $60\,\mathrm{mm}$ in lenght,
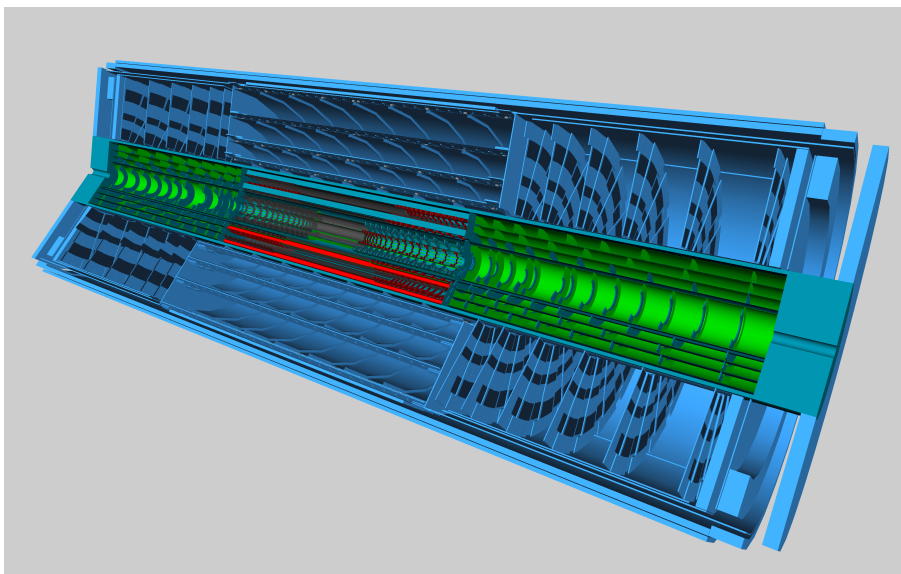

Figure 1. 3D model of the new ATLAS Inner Tracker. (Image from Ref. [4], © 2018 CERN, CC BY 4.0)

depending on their position in the detector, and have a distance between strips, called the *pitch*, of around $75\,\mu$m. In order to regain some of the spatial resolution along the lenght of the strips, the sensors are installed in so-called stereo modules, where two sensors are positioned in a pair and rotated by a small angle relative to each other [5]. This enables two hits per particle crossing in a layer, with the point of crossing at the intersection of the two strips that recorded a hit.

Installed closest to the interaction point, the central part of the Inner Tracker will be the Pixel Detector [4]. With a pixel pitch of either $50 \times 50\,\mu$m^2 or $25 \times 100\,\mu$m^2 [4], these sensors will provide accurate spatial measurements used in track and vertex reconstruction.

The technology of detector fabrication being used in the new Inner Tracker is the so-called hybrid detector. This is a well-established technology, used over many years in detector design for particle physics. The main characteristic of the hybrid detector is the implementation of sensing and read-out structures on separate silicon dies. These two dies are later electrically connected with tiny solder balls, one for each pixel, in a procedure called bump bonding. Due to the small size of the bumps and consequential small tolerances for alignment, bump bonding is a slow and difficult procedure which requires special techniques and equipment, as it is rarely used for industrial purposes. It is therefore one of the major factors affecting the price and speed at which the modules can be produced [4].

2.2 Monolithic detector option

Due to the above mentioned limitations, other fabrication technologies have been considered which would reduce the complexity and cost of production. Naturally, utilizing well-established large-scale commercial processes would be an inviting solution. The standard fabrication technology being used in industry is complementary metal-oxide-semiconductor (CMOS), a method of using pairs of p-type and n-type metal-oxide-semiconductor field effect transistors to construct logic gates.

In CMOS technology, sensors can be fabricated to contain both sensing and read-out electronics on a single silicon die, thus creating a *monolithic* detector. This type of detector is particularly attractive, as it completely removes the need for bump bonding to connect the sensing and read-out components. The production process could therefore potentially be far less complex and, due to the use of well-established industrial methods, cheaper and faster to produce than hybrid detectors. The increase of production speed is also helpful in the development phase, as it decreases the time between different prototypes. Another advantage is a smaller collective amount of material being installed in the detector, which reduces the uncertainty on hit position due to multiple scattering.

For these reasons, the ITk development group has been assessing the potential for using monolithic chips in the outermost layer of the Pixel Detector. It is in this layer that monolithic technology would benefit the most because it is the largest by area and thus requires the most amount of modules. Monolithic detectors have been used in experiments before, one example being the ALICE experiment [6], but at around two orders of magnitude lower fluence requirements and lower particle rates than the ATLAS experiment after the upgrade. The choice of the outermost pixel layer is hence also appropriate from the aspect that it is furthest from the interaction point and receives the least amount of radiation. Nevertheless, demonstrating that monolithic detectors can perform in the $40\,$MHz collision rate of the LHC and withstand the large fluences accumulated over many years of operation is an important milestone.

In recent years, a lot of research has been done in the form of design options together with performance and radiation hardness evaluations to produce a monolithic pixel detector for the Phase-II upgrade (see for example Refs. [7] and [8]). It is also the topic of this article to focus on radiation damage and its effects on detector performance.

3. Radiation damage in silicon detectors

3.1 p-n junction

In the simplest terms, silicon detectors are diodes with a voltage applied in the reverse direction. The detector contains a junction of p- and n-type doped silicon, at which a depleted region forms, containing no majority charge carriers. The depleted region has a nonzero charge density, resulting in an electric field accros it and a corresponding potential difference. Since the charge density is known, this potential difference can be calculated from the Poisson equation. By assuming an abrupt junction, with an exact boundary between the two materials, and a planar configuration, which makes the problem one-dimensional, the potential difference is

$$V = \frac{e_0}{2\varepsilon\varepsilon_0} \left(N_{\mathrm{D}} x_{\mathrm{n}}^2 + N_{\mathrm{A}} x_{\mathrm{p}}^2 \right) , \tag{3}$$

where N_{D} and N_{A} are concentrations of donor and acceptor atoms, respectively, $x_{\mathrm{p,n}}$ are the widths of the depleted regions in p- and n-type material and ε is the relative permittivity of silicon. We also get a net neutrality condition of the depleted region

$$N_{\mathrm{D}} x_{\mathrm{n}} = N_{\mathrm{A}} x_{\mathrm{p}} . \tag{4}$$

In particle detectors, one of the two doping concentrations is usually significantly larger than the other, which results in the depletion region extending almost exclusively into the side with a lower doping concentration. We can therefore neglect the depletion depth in the heavily doped side. By inverting Eq. (3) we can express the depletion width w of the detector

$$w = \sqrt{\frac{2\varepsilon\varepsilon_0}{e_0 N_{\mathrm{eff}}} V} \tag{5}$$

and introduce an effective space charge concentration N_{eff}. This is introduced since after irradiation, the space charge concentration is no longer equal to the doping concentration, which is discussed in Sec. 3.2. By biasing the junction in the reverse direction we can increase the width of the depleted region. Under bias, the depletion width becomes

$$w = \sqrt{\frac{2\varepsilon\varepsilon_0}{e_0 N_{\mathrm{eff}}} V_{\mathrm{b}}} , \tag{6}$$

where V_{b} is the bias voltage. The inherent voltage V across the junction was neglected since the biasing voltages are usually much larger in comparison.

3.2 Effect of radiation

There are two main types of radiation that affect particle detectors. The first of these is ionising radiation, which is a result of charged particles and photons ionising the detector material and producing electron-hole pairs. Long-term effects of this type of radiation are only present in silicon oxide layers, commonly used for insulation in field effect transistors, resulting in a gradual degradation of read-out electronics. The bulk material, however, is not affected by ionising radiation [9].

The main contribution to damage in the lattice comes from non-ionising interaction in the form of displacement damage, predominantly coming from hadrons. It is a consequence of high energy particles knocking out atoms from their places in the lattice, resulting in an interstitial silicon atom and a vacancy in the lattice (also called a Frenkel pair). If the transfered energy is high enough, additional atoms can be knocked out of their respective positions, forming a cluster. Some of the Frenkel pairs recombine, while other interstitials and vacancies move through the lattice and

interact with other impurities or amongst themselves. The result of these interactions are defects which change the properties of the material and hence contribute to the radiation damage [10].

Some of these defects are electrically active and change the electrical properties of the material by introducing new energy levels in the band gap and effectively acting as donors or acceptors. These changes have some important macroscopic effects which alter detector performance.

3.2.1 Leakage current

Even when biased in the reverse direction, diodes exhibit a leakage current coming from thermal generation of electron-hole pairs in the depleted region. After irradiation, the leakage current increases due to the extra energy levels in the band gap from the radiation induced defects acting as current generation centers, the most effective being those close to the middle of the band gap [11]. The increase in the leakage current per unit volume

$$\frac{\Delta I}{V} = \alpha \Phi_{\text{eq}} \tag{7}$$

is proportional to the equivalent fluence Φ_{eq}, which is rescaled to correspond to the damage done by $1\,\text{MeV}$ neutrons. It is highly temperature dependent, thus heavily irradiated detectors can be cooled to suppress the current. If sufficient cooling is not provided, the leakage current can heat the material through ohmic heating and cause a thermal runaway. A higher leakage current also increases the noise from the detector, and thus reduces the signal to noise ratio [7], which is another reason to cool the detector.

3.2.2 Charge trapping

After the high energy particle creates electron-hole pairs in the depleted region, the created charges drift to the corresponding electrodes, producing the desired signal. The radiation defects that develop in the bulk can act as traps for these charges. If these charges are trapped for longer than the signal collection time of the electronics, they cannot contribute to the signal, which leads to a lower charge collection efficiency and therefore again to a lower signal to noise ratio [7, 11]. By increasing the received fluence, more defects are present in the material, and the probability of drifting charges getting trapped by the defects increases as well.

3.2.3 Change in effective doping concentration and acceptor removal

As mentioned in Sec. 3.2, point defects can be electrically active and act as donors or acceptors. This results in the initial doping concentration not being the only contributor to N_{eff}. The defects introduced by radiation can change N_{eff} and thus affect the depletion properties of the detector described by Eq. (6).

The majority of defects introduced with radiation act as acceptors. For n-type material, which is initially doped with donors, this has an important consequence of n-type material eventually converting to p-type after receiving a high enough fluence [11]. This effect is called type inversion.

An introduction of additional acceptors is, however, not the only mechanism changing the effective doping concetration. In addition, the original acceptors or donors introduced into silicon with doping get deactivated by means of interactions with interstitial silicon atoms, vacancies and other impurities present in the material (predominantly oxygen and carbon) [7]. This effect is called acceptor or donor removal, depending on which type of dopant gets deactivated.

By taking both effects into account, we can parameterise the dependence of the effective doping concentration N_{eff} on the received fluence. For p-type material, this means a removal of initial acceptors and a constant introduction of acceptors

$$N_{\text{eff}}(\Phi_{\text{eq}}) = N_{\text{eff},0} - N_{\text{c}} \left(1 - e^{-c\,\Phi_{\text{eq}}}\right) + g_{\text{c}} \Phi_{\text{eq}}, \tag{8}$$

where $N_c \leq N_{\text{eff},0}$ and represents the fact that initial acceptors might only be removed in part, c is the removal coefficient and g_c is the acceptor introduction rate [12]. After high values of received fluence, after the acceptor removal is completed, the last term in Eq. (8) leads to an increasing effective doping concentration. Considering Eq. (6), this is undesirable, as it leads to a higher needed voltage to deplete the detector to the same depth. At large fluences, the biasing voltage needed to fully deplete the detector can reach the limit of breakdown, at which point the detector would need to be kept underdepleted to operate properly. It is therefore preferable to have the introduction rate g_c small to slow the increase of N_{eff} and allow the detector to operate fully depleted at lower biasing voltages for longer. Since g_c depends on the impurity content in the material when irradiated with some types of particles, the rate can be somewhat controled, and oxygen enriched silicon has been seen to lower this rate for certain particle types, whereas the introduction of carbon can increase it [12].

Of all the interstitial-vacancy pairs and other consequent defects produced, some of them can be reversed to recover the lattice structure since the atoms have some thermal energy. For example, if we increase the temperature in the material, some interstitials and vacancies could recombine from the increased thermal energy they received. This process is called annealing, and affects N_{eff} as well, which is therefore dependent not only on the fluence received, but also on the temperature conditions of the environment and time spent in those conditions. If, however, the material is annealed for too long, a negative effect, called reverse annealing, is seen [11]. Therefore, an optimal annealing time exists where the beneficial effects are the greatest. Annealing is already present at room temperature, and the optimal time is about 10 days [7]. By storing the detectors at a higher temperature, the time for optimal effects can be reduced, thus a so-called standard annealing is achieved by storing the detectors at $60\,^\circ$C for 80 minutes.

4. Experimental setup and measurements

Before a silicon sensor design can be used in a large particle detector, prototypes are developed to measure their properties, determine the suitability of the design and propose possible improvements. One of the methods being used in this phase of development is the transient current technique (TCT), which uses short pulses of focused laser light to generate electron-hole pairs in the depleted region, providing a measurable signal on the output. The technique can be used to study charge collection properties of detectors. It is possible to focus the laser light down to a width smaller than the size of the detector pixel, thus allowing positionally dependent measurements.

The last feature is particularly useful if we orient the laser to probe the detector from the side, i.e. parallel with the p-n interface. This method is called Edge-TCT [13], as the laser light is probing the edge of the detector as opposed to its front side, which is called Top-TCT. Positional Edge-TCT measurements are particularly useful as they can provide information about the depletion width of the detector. By measuring the charge collected by the sensor after a laser pulse at different laser beam positions in the pixel, we can estimate the size of the depleted region, since the charges created outside the depleted layer will not drift towards the electrodes and will therefore not contribute to the collected charge.

In the experimental setup, the laser light is guided though an optical fiber towards a focusing lens that achieves a beam width of about $10\,\mu$m at its narrowest point. The prototype detectors studied in this work are made by LFoundry in $150\,$nm CMOS technology with a pixel size of $60\,\mu$m [14]. A schematic view of the pixel cross section is shown in Fig. 2. At the surface, p-type and n-type transistors are embedded in the PWELL and NWELL regions and form the CMOS read-out logic, while the sensing part is located deeper, between the DNWELL and p-substrate layers. This configuration therefore fulfills the monolithic detector design requirements. For determining charge
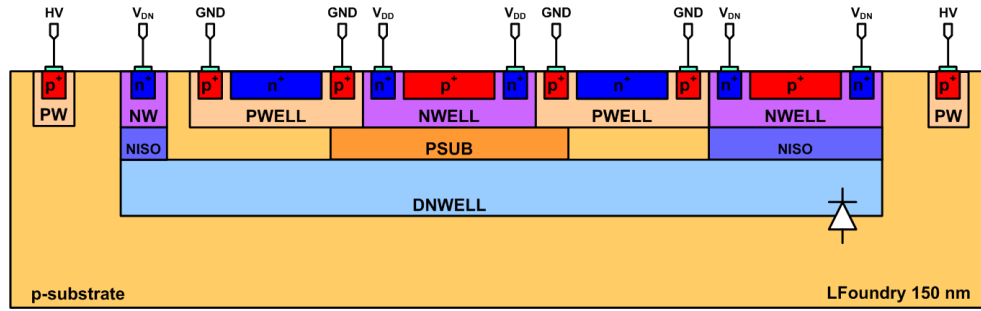
Figure 2. Simplified schematic pixel cross section of the prototype LFoundry detector. The depleted region is created on the interface of the p-substrate and DNWELL layers. On the surface, the CMOS logic structures can be seen. The intervening layers provide isolation of the CMOS logic from the sensing volume. (Image from Ref. [14])
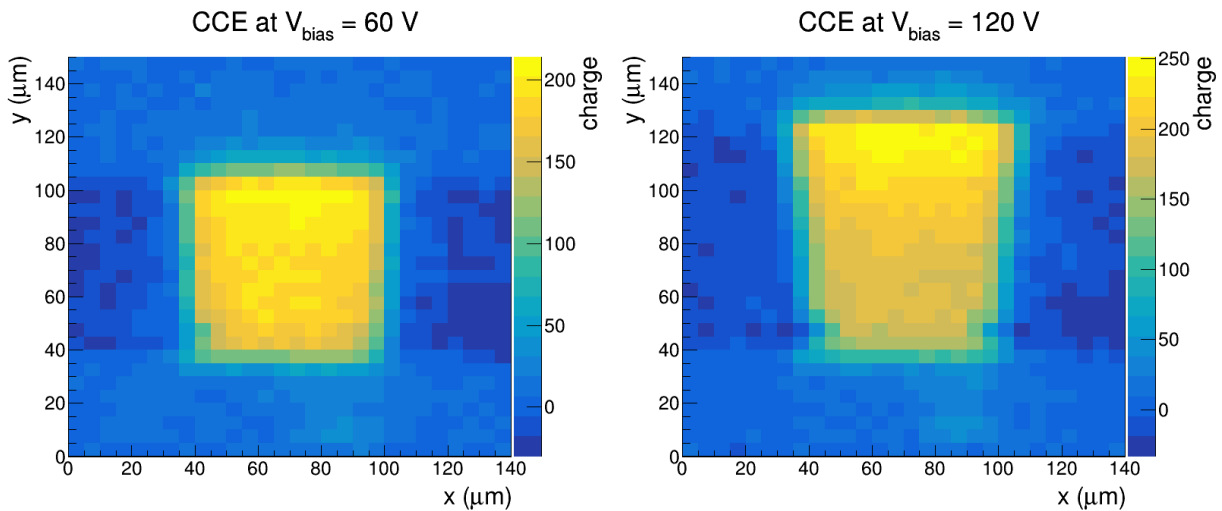

Figure 3. 2D Edge-TCT scans of a depleted pixel at two different biasing voltages. The charge is calculated by integrating the output signal within a fixed time interval. The chip surface is at $y = 40\,\mu$m. The increase of the depletion width at a higher biasing voltage is clearly evident.

collection properties, test structures on the prototype chips are used, comprising of a 3×3 grid of pixels. These test structures do not have read-out logic transistors implemented in the P- and NWELLs, and the signal therefore comes from the sensing electrode, later being amplified by an external amplifier. The prototype chip is mounted on a support and a biasing voltage is applied to deplete the detector. After each light pulse, the signal is first amplified and then measured with an oscilloscope. To reduce the noise, signals from several light pulses are averaged together.

By utilizing the ability of the setup to perform positional measurements, we can firstly conduct a two-dimensional scan of the area around the depleted region. By recording the charge collected by the electrode at each laser position, we can plot a two-dimensional distribution of the charge collection region and therefore the depleted region. An example of such a measurement with a single pixel biased at two different voltages is presented in Fig. 3. The depleted area is clearly visible, measuring $60\,\mu$m across as expected from the size of each pixel. The depth of the depleted region depends on the biasing voltage via Eq. (6) and is greater for the larger biasing voltage.

From the above scans it is evident that the depletion width of the pixel can be determined though the measurement of the collected charge. This in turn gives us the ability to compute the effective space charge concentration N_{eff}. To perform this measurement, we run charge collection scans over the entire width of the depleted region through the center of the pixel. In the example of Fig. 3, this would result in scans in the y-direction at approx. $x = 70\,\mu$m. Then the width of the depleted region is estimated. In the following results, the full width at half maximum (FWHM)
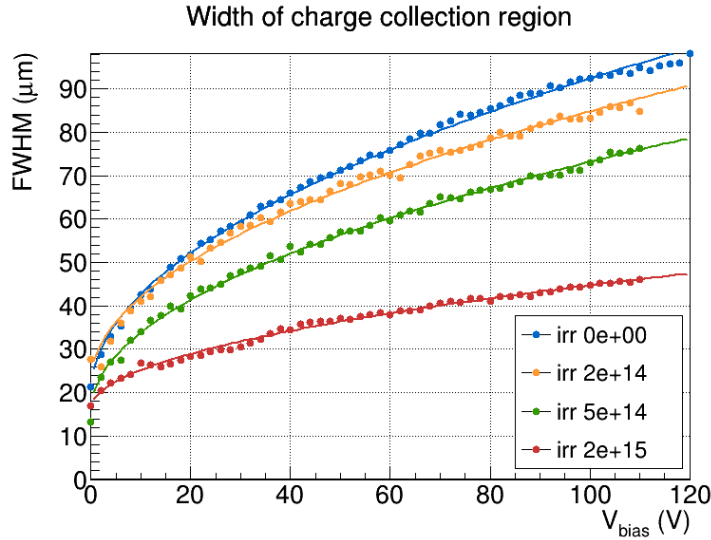
Figure 4. The width of the depleted region as a function of the applied bias voltage for different irradiation fluences. At high fluence values, the depletion width is significantly smaller at a fixed bias voltage.

of the charge collection profile was used as the depletion width. These scans can be performed at different biasing voltages to get the full dependence of the width on the bias voltage. Sample results for these measurements are shown in Fig. 4, showing that we indeed get a square root proportionality between the two quantities. To extract N_{eff}, we fit the function

$$w = w_0 + \sqrt{\frac{2\varepsilon\varepsilon_0}{e_0 N_{\text{eff}}} V_{\text{b}}} \tag{9}$$

to the data. The extra term w_0 is a result of the detector already being partly depleted without a bias voltage applied, the laser beam having a finite width and the collection of charges via diffusion from the surrounding undepleted region [7].

The main result of interest is the dependence of N_{eff} on the received fluence Φ_{eq}. To achieve this, identical samples are irradiated to different fluences, up to the values expected in the outer layer of the Pixel Detector after the HL-LHC upgrade. In this case, neutrons from the TRIGA nuclear reactor in Ljubljana [15, 16] were used. We can then perform depletion depth measurements for each fluence level, as shown in Fig. 4. We are interested in the relation $N_{\text{eff}}(\Phi_{\text{eq}})$ from Eq. (8) and by plotting this (example in Fig. 5), we can fit Eq. (8) to the data and extract the parameters of the model. These can tell us when the initial acceptor removal is completed and how the effective doping concentration changes afterwards, when the dominant contribution comes from the linear term. With this, vital information is gained about how the detector will perform throughout the entire expected lifetime of operation.

5. Conclusion

The silicon particle detector is an essential part of many particle physics experiments. Since the path to higher luminosities results in harsher conditions for the detectors, the development of new prototypes being able to cope with such conditions is necessary. To produce a well performing radiation hard detector, a good understanding of the processes causing radiation damage in silicon is required, as well as how they impact detector performance. Through experimental techniques, such as Edge-TCT measurements, the specific properties of the individual prototype being developed can be determined, thus helping to provide important information in developing an adequate silicon detector for a particle physics experiment.
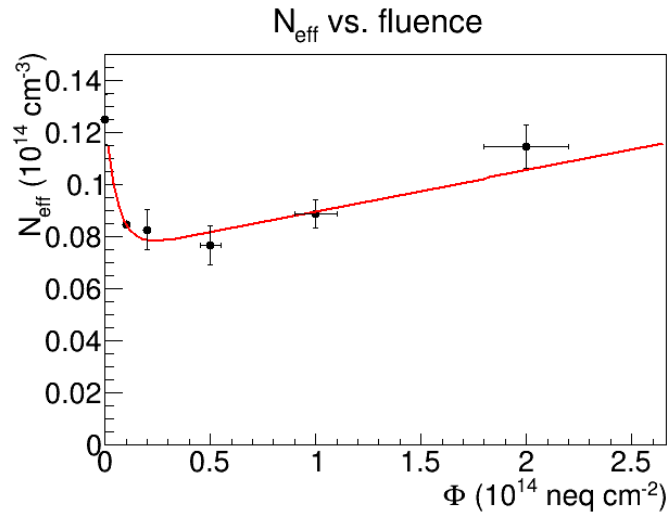
Figure 5. Example of the measured change in N_{eff} for different neutron fluences. By fitting the model from Eq. (8), we can extract the relevant parameters.

REFERENCES

[1] ATLAS Collaboration, *The ATLAS Experiment at the CERN Large Hadron Collider*, Journal of Instrumentation **3** (2008), S08003.

[2] I. Béjar Alonso, O. Brüning, P. Fessia, L. Rossi, L. Tavian and M. Zerlauth, *High-Luminosity Large Hadron Collider (HL-LHC): Technical Design Report*, CERN Yellow Reports: Monographs, 2020.

[3] ATLAS Collaboration, *Letter of Intent for the Phase-II Upgrade of the ATLAS Experiment*, Tech. Rep. CERN-LHCC-2012-022, LHCC-I-023, 2012.

[4] ATLAS Collaboration, *Technical Design Report for the ATLAS Inner Tracker Pixel Detector*, Tech. Rep. CERN-LHCC-2017-021, ATLAS-TDR-030, 2017.

[5] ATLAS Collaboration, *Technical Design Report for the ATLAS Inner Tracker Strip Detector*, Tech. Rep. CERN-LHCC-2017-005, ATLAS-TDR-025, 2017.

[6] P. Yang, G. Aglieri, C. Cavicchioli, P. L. Chalmet, N. Chanlek, A. Collu, C. Gao, H. Hillemanns et al., *MAPS Development for the ALICE ITS Upgrade*, Journal of Instrumentation **10** (2015), C03030.

[7] B. Hiti, *Radiation Hardness of CMOS Detector Prototypes for ATLAS Phase-II ITk Upgrade*, Ph.D. thesis, University of Ljubljana, Faculty of Mathematics and Physics, 2020.

[8] A. Affolder, M. Andelković, K. Arndt, R. Bates, A. Blue, D. Bortoletto, C. Buttar, P. Caragiulo et al., *Charge Collection Studies in Irradiated HV-CMOS Particle Detectors*, Journal of Instrumentation **11** (2016), P04007.

[9] M. Garcia-Sciveres and N. Wermes, *A Review of Advances in Pixel Detectors for Experiments with High Rate and Radiation*, Reports on Progress in Physics **81** (2018), 066101.

[10] F. Hönniger, *Radiation Damage in Silicon: Defect Analysis and Detector Properties*, Ph.D. thesis, Universität Hamburg, 2007.

[11] M. Moll, *Displacement Damage in Silicon Detectors for High Energy Physics*, IEEE Transactions on Nuclear Science **65** (2018), 1561–1582.

[12] G. Lindström, M. Ahmed, S. Albergo, P. Allport, D. Anderson, L. Andricek, M. Angarano, V. Augelli et al., *Radiation Hard Silicon Detectors—Developments by the RD48 (ROSE) Collaboration*, Nuclear Instruments and Methods in Physics Research Section A: Accelerators, Spectrometers, Detectors and Associated Equipment **466** (2001), 308–326.

[13] G. Kramberger, V. Cindro, I. Mandić, M. Mikuž, M. Milovanović, M. Zavrtanik and K. Žagar, *Investigation of Irradiated Silicon Detectors by Edge-TCT*, IEEE Transactions on Nuclear Science **57** (2010), 2294–2302.

[14] *RD50-MPW2 Documentation*, 2019.

[15] L. Snoj, G. Žerovnik and A. Trkov, *Computational analysis of irradiation facilities at the JSI TRIGA reactor*, Applied Radiation and Isotopes **70** (2012), 483–488.

[16] K. Ambrožič, G. Žerovnik and L. Snoj, *Computational analysis of the dose rates at JSI TRIGA reactor irradiation facilities*, Applied Radiation and Isotopes **130** (2017), 140–152.